Acta Scientiarum

http://periodicos.uem.br/ojs
ISSN on-line: 1807-8664
Doi: 10.4025/actascitechnol.v44i1.60386





# Premature ventricular contraction recognition using blind source separation and ensemble gaussian naive bayes weighted by analytic hierarchy process

**Bruno Rodrigues de Oliveira[1*], Marco Aparecido Queiroz Duarte[2] and Jozue Vieira Filho[3]**

[1]Departamento de Engenharia Elétrica, Universidade Estadual Paulista "Júlio de Mesquita Filho", Av. Brasil, 56, 15385-000, Centro, Ilha Solteira, São Paulo, Brasil. [2]Curso de Matemática, Universidade Estadual de Mato Grosso do Sul, Cassilândia, Mato Grosso do Sul, Brasil. [3]Engenharia Eletrônica e de Telecomunicações e Engenharia Aeronáutica, Universidade Estadual Paulista "Júlio de Mesquita Filho", São João da Boa Vista, São Paulo, Brasil. *Author for correspondence. E-mail: bruno@editorapantanal.com.br

**ABSTRACT.** Premature Ventricular Contractions (PVC) arrhythmias can be associated with sudden death and acute myocardial infarction, occurring in 50% of the population for Holter monitoring. PVC patterns are very hard to be recognized since their waveforms can be confused with other heartbeats, such as Right and Left Bundle Branch Blocks. This work proposes a new approach for PVC recognition, based on Gaussian Naive Bayes algorithm and AMUSE (Algorithm for Multiple Unknown Signal Extraction), which is a method for the blind source separation problem. This approach provides a set of attributes that are combined by Linear Discriminant Analysis, allowing the training of an ensemble learning. The Analytic Hierarchy Process weights each learned model according to its importance, obtained from the performance metrics. This approach has some advantages over baseline methods since it does not use a pre-processing stage and employs a simple machine learning model trained using only two parameters for each feature. Using a standard dataset for training and test phases, the proposed approach achieves 98.75% accuracy, 90.65% sensitivity, and 99.46% specificity. The best performance was 99.57% accuracy, 98.64% sensitivity, and 99.65% specificity for other datasets. In general, the proposed approach is better than 66% of the state-of-the-art methods concerning accuracy.

**Keywords:** Arrhythmia recognition; ensemble learning; machine learning; heart diseases; decision making in health.

Received on August 1, 2021.
Accepted on November 2, 2021.

## Introduction

Normal heart rhythm is controlled regularly by the sinus (SA) node located in the right atrium using cell depolarization. Whether the sinoatrial node depolarization is insufficient to supplant other cardiac cells depolarization, or there is a blockage in the electrical impulse conduction in the atrioventricular (AV) node, then another cardiac cell may assume the heart rhythm (Hall, 2015; Bennett, 2012). If the ectopic focus is situated below the AV node, then a Premature Ventricular Contraction (PVC) is characterized, and the ventricles may assume the pacemaker function. This is also due to reentry, when an electrical impulse generated in the ventricles returns to them, either due to a shortened refractory period or to an elongation of the ventricular fiber, that makes the impulse travel a longer path (Ahn, 2013; Latchamsetty & Bogun, 2015; Cha, Lee, Klarich, & Grogan, 2012).

PVC are not always associated with heart disease. They can also be caused by lack of sleep, irritability, coffee, and drugs (Garcia & Miller, 2004). They are considered benign if the patient has no structural heart disease. If PVC occurrences are high, hemodynamic problems may occur. They are also indicator of some reentry mechanism existence resulting from infarcted or ischemic areas. This can lead to an increased risk of lethal Ventricular Fibrillation (VF) or even sudden death (Hadia et al., 2017; Ahn, 2013; Kusumoto, 2009; Garcia & Miller, 2004). PVC are also associated with an increased risk of Atrial Fibrillation (AF) (Kim, Han, Choi, Choi, Choi, Shim, & Kim, 2021a), heart failure, and ventricular tachyarrhythmia (Kim, Choi, Han, Min, Choi, Shim, Choi, & Kim, 2021b).

PVC prevalence had been estimated in a study of 301 middle-aged men, where 62% were diagnosed with some ventricular arrhythmia, including PVC (Latchamsetty & Bogun, 2015). For those individuals who were

at high risk of coronary artery disease, PVC occurrence was more frequent. In another study with more than 122,000 military men, mostly young and healthy, PVC occurrence was lower than 1% (Latchamsetty & Bogun, 2015). It is estimated that PVC prevalence occurs from 20% to 30% of the general population. For 24-hour or 48-hour Holter monitoring, this percentage rises to 50% of the population (Kusumoto, 2009). On the other hand, for a simple ECG, such occurrence is reduced from just 1% to 4% in the general population (Latchamsetty & Bogun, 2015). In another study, the authors found that the prevalence of PVC-cardiomyopathy was 29% of the general population (Huizar et al., 2021).

The Electrocardiogram (ECG) measures the electrical heart activity using electrodes (sensors) placed on the chest, arms, and legs. It comprises three waveforms, which representes the atrial depolarization (P wave), ventricular depolarization (QRS complex), and ventricular repolarization (T wave).

PVC have their own electrocardiograph characteristics, such as: a) Absence of the P wave preceding the QRS complex; b) Extended QRS complex (greater than 0.12 seconds), which may have a bizarre appearance and high voltage; c) QRS complex with the right (RBBB) and left bundle branch block (LBBB) appearance, when the extrasystole comes from the right or left ventricle, respectively; d) Polarity of T wave and ST-segment opposite to QRS complex; e) Premature QRS complex (Garcia & Miller, 2004; Hadia et al., 2017).

Given the multiplicity of PVC patterns due to electrocardiographic characteristics, and the need for longer examinations such as Holter, the proposition of mathematical/computational tools is critical to help the specialists in the PVC recognition task. Some of these propositions and their methodologies are mentioned below.

Inan, Giovangrandi, and Kovacs (2006) proposed the use of the Wavelet Transform (WT) to generate the feature vectors for training a neural network (NN) with six sets of spectral features, obtained from five decomposition levels and one temporal attribute, obtained by the normalized ratio between the RR intervals. Shen, Hu, Li, and Meng (2011) implemented three different methodologies for extracting six attributes, which were divided into temporal, frequency, and morphological, and employed the support vector machine (SVM) with a radial basis function as the kernel. Adnane and Belouchrani (2013) proposed a threshold method to determine clusters belonging to PVC beats. Bazi, Hichri, Alajlan, & Ammour (2013) implemented a feature extraction method using four WT decomposition levels, S-Transform, and morphological criteria, and to PVC classification employed gaussian process classifiers. Li et al. (2014) presented a model-based approach using morphological differences between ventricular depolarization and repolarization phases. Liu, Du, Wang, Zhou, and Zhang (2015) proposed a new set of features based on Lyapunov exponents and their derivatives and the NN vector quantization. Zarei, He, Huang, and Zhang (2016) proposed a scheme based on the variation of the principal directions from the Principal Component Analysis by building a matrix with non-PVC and PVC heartbeats. Hadia et al. (2017) implemented a methodology to detect PVC based on morphological characteristics of the ECG and, for PVC classification, proposed the K-nearest-neighbors with five neighbors. Zhou, Jin, and Dong (2017) presented a new methodology combining deep neural networks (lead convolutional NN and long short-term memory) and inference rules based on signal quality judgment for PVC recognition. Oliveira, Abreu, Duarte, and Vieira Filho (2019) proposed a new set of features inspired by geometric figures constructed over QRS complexes and various machine learning algorithms such as: multinomial naive Bayes, voted perceptron, NN, SVM, Radial-basis functions network, random forest (RF) and artificial immune systems. Xie et al. (2019) proposed a combination of features such as RR, PR, QRS and QT intervals, QRS area, and R wave amplitude, using RF with CART algorithm for PVC classification.

However, PVC recognition is very hard task due to its dissimilarity, as observed in Oliveira et al. (2019), since the same heartbeat type can have very different characteristics. Examples are the LBBB and RBBB heartbeats. As mentioned earlier, PVC may look like these heartbeats (Garcia & Miller, 2004; Hadia et al., 2017), but LBBB and RBBB belong to a standard class, according to the Association for the Advancement of Medical Instrumentation (AAIM)[1]. On the other hand, PVC belongs to the ventricular ectopic class. In addition, in Oliveira, Duarte, and Vieira Filho (2022) the authors found that the LBBB, RBBB, and Normal heartbeats have enough differences to recognize them in distinct classes. Therefore, any PVC recognition approach must be able to avoid these confusions.

This work presents a new method for feature extraction based on AMUSE (Algorithm for Multiple Unknown Signal Extraction) blind source separation method without performing any pre-processing stage, followed by Linear Discriminant Analysis (LDA) to combine the features and reduce the dimensionality. The use of AMUSE is justified since the ECG can be seen as a superposition of heart activities, which this algorithm can separate.

[1] Practice for Testing and Reporting Performance Results of Ventricular Arrhythmia Detection Algorithms. 1987.

The new set of features is used for the PVC recognition task through an ensemble method that builds over the Gaussian Naive Bayes (GNB), where each induced model is weighted using Analytic Hierarchy Process (AHP). The model's weight is set according to its performance and a conversion function that converts the performance difference into a scale used in the AHP framework.

## Materials and methods

Let $\boldsymbol{A}_0 \in \mathbb{R}^{N\times M}$ be a mixing environment with $N$ sensors and $M$ sources, with $M \leq N$. The observed signals are given in the matrix $\boldsymbol{X} = \boldsymbol{A}_0\boldsymbol{S} + \boldsymbol{V}$, where $\boldsymbol{S} \in R^{M\times P}$ and $\boldsymbol{V} \in \mathbb{R}^{N\times P}$ are stationary zero-mean sources and noise matrices, respectively; $P$ is the length of the signals. $\boldsymbol{V}$ is defined as a white noise process with covariance matrix $\boldsymbol{R}_V = \sigma^2\boldsymbol{I}$.

To estimate latent sources in $\boldsymbol{S}$ from the observed signals in $\boldsymbol{X}$, AMUSE is employed applying the steps (Tong, Liu, Soon, & Huang, 1991): i) estimate the covariance matrix $\boldsymbol{R}_{\boldsymbol{X}}$ using the Eigendecomposition $\boldsymbol{R}_{\boldsymbol{X}} = \boldsymbol{L}\boldsymbol{\Psi}^2\boldsymbol{L}^\intercal + \sigma^2\boldsymbol{I}$ where $\boldsymbol{\Psi} = \text{diag}(\psi_1^2, \cdots, \psi_N^2)$ is a diagonal matrix composed by the eigenvalues and $\boldsymbol{L}$ is a matrix where its columns are the eigenvectors; ii) obtain an orthogonalization transformation $\mathcal{T} = \boldsymbol{\Psi}^{-1}\boldsymbol{L}^\intercal$; iii) project $\boldsymbol{X}$ onto orthogonal space $\boldsymbol{Y}$ using $\mathcal{T}$; iv) compute the Eigendecomposition for the symmetric covariance matrix $\boldsymbol{R}_{\boldsymbol{Y}_{sym}}$ for a given delay $\tau$ in the equation $\boldsymbol{R}_{\boldsymbol{Y}_{sym}} = (\boldsymbol{R}_{\boldsymbol{Y}}(\tau) + \boldsymbol{R}_{\boldsymbol{Y}}(\tau)^\intercal)/2$, where $\boldsymbol{R}_{\boldsymbol{Y}}(\tau) = \text{E}\{\boldsymbol{Y}(p)\boldsymbol{Y}(p-\tau)^\intercal\}$, $\text{E}\{\cdot\}$ is the expectation, $\boldsymbol{Y}(p) = [y_1(p)\ y_2(p) \cdots y_M(p)]^\intercal$, $p = 1,2,\cdots,P$, and $y_m(p)$ is the $m$-th orthogonal signal (source); v) build an unmixing matrix $\boldsymbol{B}$ with the vectors obtained in the last step from $\boldsymbol{R}_{\boldsymbol{Y}_{sym}}$; vi) estimate the sources using $\widehat{\boldsymbol{S}} = \boldsymbol{B}^\intercal\boldsymbol{Y}$ (Tong et al., 1991).

Let $\text{T} = (\boldsymbol{x}_k, y_k)_{k=1}^K$ be a dataset with $K$ instances; $\boldsymbol{x}_k = [x(1)\ x(2) \cdots x(Q)]$ has $Q$ features and the classification is $y_k \in \{0, 1\}$, where 0 and 1 encode two classes of patterns. To learn a decision boundary to separate these patterns, in a supervised way, T is split into two datasets: Tr for training/induction and Te for test/validation. Gaussian Naive Bayes (GNB) is one of the most popular and low-cost machine learning algorithms. It is based on three assumptions: i) Bayes rule $p(y|\boldsymbol{x}) = p(\boldsymbol{x}|y)p(y)/p(\boldsymbol{x})$, where $p(\boldsymbol{x})$ and $p(y)$ are prior probabilities, $p(y|\boldsymbol{x})$ and $p(\boldsymbol{x}|y)$ are posterior probabilities; ii) statistical independence of features, i.e., $p(\boldsymbol{x}|y) = \prod_{q=1}^{Q} p(x(q)|y)$; iii) features are normally distributed, so that the probabilities are given by density function (1), for each feature $q$.

$$p(x(q)|y_k) = \frac{\exp\left[-\frac{\left(x(q) - \mu_{qk}\right)^2}{2\sigma_{qk}^2}\right]}{\sqrt{2\pi\sigma_{qk}^2}}, \tag{1}$$

where $\mu_{qk}$ and $\sigma_{qk}$ are estimated in the induction phase for each $y_k$ class and $\exp(\cdot)$ is the exponential function.

A $Q$-dimentional $\boldsymbol{x}_k$ pattern can be projected in a lower dimension space through Linear Discriminant Analysis, combining vectors of features linearly, so $\boldsymbol{z}_k = \boldsymbol{u}^\intercal\boldsymbol{x}_k$, where $\boldsymbol{u}$ is a weight vector. The estimation of $\boldsymbol{u}$ is based on maximizing $J(\boldsymbol{u}) = \boldsymbol{u}^T\boldsymbol{Z}_B\boldsymbol{u}/\boldsymbol{u}^T\boldsymbol{Z}_U\boldsymbol{u}$, where $\boldsymbol{Z}_U$ and $\boldsymbol{Z}_B$ are within classes scatter and between types scatter matrices, respectively (Mika, Ratsch, Weston, Scholkopf, & Mullers, 1999).

Analytic Hierarchy Process (AHP) is a method for decision making proposed by Saaty (Saaty, 1987; Santos, Neves, Sant'Anna, Oliveira, & Carvalho, 2019) and extensively used in the most diverse areas (Ho & Ma, 2018; Santos et al., 2019). In this hierarchy model, at the top and the bottom, there are put a goal and the alternatives, respectively, and in the middle the criteria used to compare the alternatives. This comparison results in a square pairwise matrix $\boldsymbol{A}_l = \left(a_{ij}\right) \in \mathbb{Q}^{D\times D}$, where $D$ is the number of alternatives and $l$ a criterion. The main diagonal elements in $\boldsymbol{A}_l$ are equal to one, and the others are $a_{ij} = 1/a_{ji}$, where $a_{ij} = w_i/w_j$ is the judgment value of alternative $i$ over alternative $j$ for some criterion. The verbal judgment is employed using the Saaty's scale described in Table 1. If the decisions are consistent, then the determinant of $\boldsymbol{A}_l$ is zero (Oliveira, Oliveira, Freitas, & Duarte, 2021). A judgment is consistent if an alternative $A_1$ is preferable over $A_2$, and the latter is preferable over $A_3$, then $A_1$ is preferable over alternative $A_3$. In the case of consistency, there is only one nonzero eigenvalue from $\boldsymbol{A}$, named $\lambda_{max}$ (Saaty, 1987; Santos et al., 2019; Oliveira et al., 2021).

The eigenvector gives the judgments scores (importance) $\boldsymbol{w}_l = [w_{1l}, w_{2l}, \cdots, w_{Dl}]^\intercal$ related to the higher eigenvalue $\lambda_{max}$ from $\boldsymbol{A}_l$. Local priority is provided by $w_{li}$ concerning the $l$-th criterion. The global priority vector, obtained from all judgments, is given by $\boldsymbol{v} = [v_1, v_2, \cdots, v_D]^\intercal$, where

$$v_p = \sum_{l=1}^{L} s_l w_{pl} \quad (2)$$

for $p = 1,2,\cdots,D$, where $w_{pl}$ is the local priority of alternative $p$ concerning the $l$-th criterion and $s_l$ is the $l$-th criterion weight. Commonly $\boldsymbol{v}$ is normalized, i.e., $\sum v_p = 1$ (Santos et al., 2019).

**Table 1.** Saaty's scale.

| Verbal judgment | Importance value |
|---|---|
| Equal importance | 1 |
| Somewhat more importance | 3 |
| Much more important | 5 |
| Very much more important | 7 |
| Absolutely more important | 9 |
| Intermediate value (weaker) | 2, 4, 6, 8 |

## Results

An overview of the proposed approach[2] is illustrated in Figure 1. The data flow is applied to each ECG register in the database, as follows:

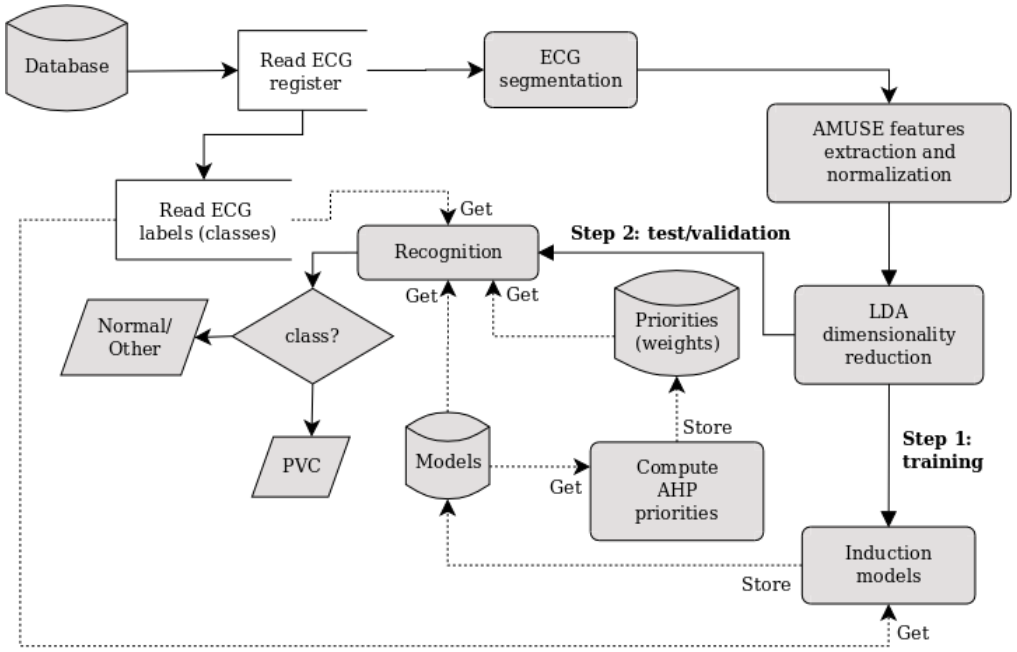


**Figure 1.** Block diagram of the proposed approach. Solid and dotted lines mean: data flow and actions on the data, respectively.

(1) ECG segmentation: segments are obtained in the following way: $\boldsymbol{x}_k(m) = \boldsymbol{x}(p), R_k - J_l\nabla \leq p \leq R_k + J_r\nabla$, where $\nabla$ is the ECG sampling rate (Hz), $J_l$ and $J_r$ are the left and the right lengths (in seconds) for a rectangular window, where $J_l = J_r$ such that $J_l + J_r = 0.75$, where 0.75 is the average duration in seconds of a cardiac cycle, $p = 0,1,\cdots,P-1$; $m = 0,1,\cdots,(J_l + J_r)\nabla - 1$; $k = 1,2,\cdots,\#R$; $R_k$ is the position (to the entire ECG) for the $k$-th R wave peak; and $\#R$ is the amount of these waves.

(2) AMUSE features extraction and normalization: AMUSE application is proposed since the ECG is composed by the superposition of the electrical activity in the cardiac cells arranged in distinct sites, among them: SA node, AV node, and Purkinje system, due to depolarization and repolarization phases having different periods. AMUSE separates the low-frequency and high-frequency components, generating better-suited features for classification. However, AMUSE waits for a matrix of sources but the $k$-th ECG segment $\boldsymbol{x}_k(m)$ is a vector with a dimension equal to $(J_l + J_r)\nabla - 1$. To circumvent this inconsistency, for each $k$ segment, a matrix (3) is built:

[2] The source code is available on github (https://github.com/brunobro/Premature-Ventricular-Contraction-Recognition).

$$\boldsymbol{Y}_k = \begin{bmatrix} \boldsymbol{x}_k(0) & \cdots & \boldsymbol{x}_k\big((J_l + J_r)\nabla - 2\big) \\ \boldsymbol{x}_k(1) & \cdots & \boldsymbol{x}_k\big((J_l + J_r)\nabla - 1\big) \end{bmatrix}, \tag{3}$$

whose second row is a delayed version of the first row. This delay is necessary since the AMUSE calculates the covariance matrix, which would be null without such delay. Due to the $\boldsymbol{Y}_k$ matrix form and the orthogonality of $\boldsymbol{B}^{\mathrm{T}}$, the estimated sources will have characteristics of low ($\widehat{\boldsymbol{S}}_k[0,:]$)[3] and high ($\widehat{\boldsymbol{S}}_k[1,:]$) frequency signals. Ultimately, the sources (features) $\widehat{\boldsymbol{S}}_k$ for $k$-th segment are normalized.

(3) LDA dimensionality reduction: the features $\widehat{\boldsymbol{S}}_k[0,:]$ and $\widehat{\boldsymbol{S}}_k[1,:]$ are linearly combined by LDA, resulting in the dimensionality reduction of the input space. This reduction ensures that less relevant attributes are attenuated.

(4) Induction models: to train the models for PVC recognition, $Q$ instances are used in the dataset $\mathrm{Tr} = \big(a_q, b_q\big)_{q=1}^{Q}$, where $a_q \in \{\widehat{\boldsymbol{S}}_q[0,:], \widehat{\boldsymbol{S}}_q[1,:]\}$ and $b_q$ is the instance label (class). This approach results in two models whose outputs (predictions) are combined using weighted voting scheme.

(5) Compute AHP priorities: since each model disagrees with certain predictions, AHP application is proposed to weight these models. In the hierarchy, the goal is "choose a model", subject to criteria, namely accuracy, positive and negative predictive, sensitivity and specificity. The alternatives are the models themselves. To obtain the preferences of models in relation to some criterion, it is proposed a conversion function (6) based on Oliveira et al. (2019), which converts the difference of the metric $c_m$ generated by models $\mathcal{M}_i$ and $\mathcal{M}_j$, i.e., $c_{m,\mathcal{M}_i}$ and $c_{m,\mathcal{M}_j}$, to Saaty's scale:

$$d_{m\mathcal{M}_i\mathcal{M}_j} = \left(c_{m\mathcal{M}_i} - c_{m\mathcal{M}_j}\right)\kappa \tag{4}$$

$$\delta_{m\mathcal{M}_i\mathcal{M}_j} = \begin{cases} 1, \text{if } \left|d_{m\mathcal{M}_i\mathcal{M}_j}\right| < 1 \\ 9, \text{if } \left|d_{m\mathcal{M}_i\mathcal{M}_j}\right| > 9 \\ \left\lceil \left|d_{m\mathcal{M}_i\mathcal{M}_j}\right| \right\rceil, \text{otherwise} \end{cases} \tag{5}$$

$$\Delta_{m\mathcal{M}_i\mathcal{M}_j} = \delta_{m\mathcal{M}_i\mathcal{M}_j}^{\ \mathrm{sgn}(d_{m\mathcal{M}_i\mathcal{M}_j})}, \tag{6}$$

where $m = 1,2,\cdots,D$; $D$ is the number of metrics, $\lceil\cdot\rceil$ is the ceiling function, sgn() is the signal of difference $d_{m\mathcal{M}_i\mathcal{M}_j}$ and $\kappa > 0$ is a constant used to increase the difference. After computing the pairwise matrices, whose elements are $\Delta_{m\mathcal{M}_i\mathcal{M}_j}$, the AHP method returns a $\boldsymbol{v}$ vector with the weights for each model.

(6) Recognition: The weights in $\boldsymbol{v}$ are put in equation (7), to obtain the models weighted:

$$\hat{p}\big(y_k|a_{q'}\big) = \sum_{o=1}^{O} v_l p_l\big(y_k|a_{q'}\big), \tag{7}$$

where $O$ is the number of models[4], and $\mathrm{Te} = \big(a'_q, b'_q\big)_{q'=1}^{Q'}$ is test dataset. Finally, the ensemble output, weighted by AHP, is calculated by

$$\hat{b}_{q'} = \begin{cases} 1, \text{if } \hat{p}\big(1|\boldsymbol{a}_{q'}\big) \geq \alpha \\ 0, \text{if } \hat{p}\big(1|\boldsymbol{a}_{q'}\big) < \alpha \end{cases}, \tag{8}$$

where 0 and 1 represent Normal and PVC heartbeats, respectively, and α is a cut-off probability. Commonly $\alpha = 0.5$.

To train and test the PVC recognition models MIT/BIH-ARDB database is employed (Goldberger et al., 2000). The used datasets are described in Table 2. For performance evaluation, the following metrics are used: accuracy $A_{cc} = (TP + TN)/(TP + FP + TN + FN)$, sensibility $S_e = TP/(TP + FN)$, specificity $S_p = TN/(TN + FP)$, positive $P^+ = TP/(TP + FP)$ and negative $P^- = TN/(TN + FN)$ precisions, where $TP$ and $TN$ are true positive and negative, $FN$ and $FP$ are false positive and negative, respectively. In this work, PVC and Normal heartbeats are considered positive and the negative classes, respectively.

[3] The notation $[0,:]$ means that the first row of matrix.

[4] In order to obtain additional models just take more delayed versions in matrix $\boldsymbol{Y}_k$.

**Table 2.** Datasets used for training and testing the PVC recognition models.

| Label | ECG Registers | Instances | |
|---|---|---|---|
| | | PVC | Normal |
| D1 | 101, 106, 108, 109, 112, 114, 115, 116, 118, 119, 122, 124, 201, 203, 205, 207, 208, 209, 215, 220, 223, 230 | 3,683 | 38,087 |
| D2 | 100, 103, 105, 111, 113, 117, 121, 123, 200, 202, 210, 212, 213, 214, 219, 221, 222, 228, 231, 232, 233, 234 | 3,219 | 36,428 |
| D3 | 108, 109, 111, 112, 113, 115, 117, 122, 124, 200, 203, 207, 208, 209, 210, 212, 213, 214, 219, 222, 215, 220, 223, 228, 230, 231, 233 | 5,040 | 46,980 |
| D4 | 100, 101, 102, 103, 104, 105, 106, 107, 114, 116, 118, 119, 121, 123, 201, 202, 205, 221, 223, 232 | 2,400 | 29,826 |
| D5 | 103, 105, 106, 108, 109, 111, 112, 113, 114, 115, 116, 117, 118, 119, 121, 122, 123, 124, 200, 201, 202, 203, 205, 207, 208, 209, 210, 212, 213, 214, 215, 219, 220, 221, 222, 223, 228, 230, 231, 232, 233, 234 | 6,901 | 70,419 |
| D6 | 100, 101, 102, 104, 105, 106, 107 | 627 | 8,391 |
| D7 | 100, 102, 104, 105, 106, 107, 118, 119, 200, 201, 203, 205, 208, 212, 213, 214, 215, 217 | 4,420 | 25,124 |
| D8 | 111, 115, 116, 119, 221, 230, 231 | 953 | 10,395 |
| D9 | 106, 119, 200, 201, 208, 213, 221, 223, 233 | 4,899 | 16,930 |

In the first experiment, D1 and D2 datasets, described in Table 2, are used in training and testing phases, respectively. Two models are induced, namely $\mathcal{M}_0$ and $\mathcal{M}_1$, using the linear combination provided by LDA from the AMUSE components. $\mathcal{M}_0$ received that component associated with the higher eigenvalue, i.e., $\boldsymbol{S}_k[0,:]$, and $\mathcal{M}_1$ received the component $\boldsymbol{S}_k[1,:]$. Using the evaluation metrics, the AHP importance (weights) are obtained. The induced models and the ensemble scheme, weighted by AHP through conversion function using $\kappa = 500$, are tested, and the obtained results are shown in Table 3.

**Table 3.** First experiment results using D1 and D2 datasets for training and testing, respectively. Bold values are the best ones.

| Model | $A_{cc}$ | $S_e$ | $S_p$ | $P^+$ | $P^-$ |
|---|---|---|---|---|---|
| Single Models | | | | | |
| $\mathcal{M}_0$ | 0.9800 | 0.9214 | 0.9852 | 0.8460 | 0.9930 |
| $\mathcal{M}_1$ | 0.9777 | 0.9248 | 0.9824 | 0.8228 | 0.9933 |
| AHP ensemble approach | | | | | |
| $\alpha = 0.3$ | 0.9706 | 0.9397 | 0.9733 | 0.7566 | 0.9946 |
| $\alpha = 0.4$ | 0.9753 | 0.9292 | 0.9794 | 0.7993 | 0.9936 |
| $\alpha = 0.5$ | 0.9796 | 0.9214 | 0.9847 | 0.8419 | 0.9930 |
| $\alpha = 0.6$ | 0.9841 | 0.9158 | 0.9902 | 0.8917 | 0.9925 |
| $\alpha = 0.7$ | 0.9875 | 0.9065 | 0.9946 | 0.9374 | 0.9918 |

In the second experiment, registers are the same as for the first experiment, but the cross-validation method was employed, where for each fold, the ECG register is swapped so that each of them is in the training or testing, at least once. This approach aims to ensure the diversity of instances used in training and testing. The obtained results are shown in Table 4.

**Table 4.** Results for AHP approach with $\alpha = 0.7$ and cross-validation with 22 folds.

| Fold | $A_{cc}$ | $S_e$ | $S_p$ | $P^+$ | $P^-$ |
|---|---|---|---|---|---|
| 1 | 0.9875 | 0.9065 | 0.9946 | 0.9374 | 0.9918 |
| 2 | 0.9872 | 0.9040 | 0.9946 | 0.9378 | 0.9915 |
| 3 | 0.9870 | 0.9034 | 0.9958 | 0.9575 | 0.9899 |
| 4 | 0.9758 | 0.8541 | 0.9888 | 0.8908 | 0.9844 |
| 5 | 0.9759 | 0.8544 | 0.9891 | 0.8943 | 0.9843 |
| 6 | 0.9755 | 0.8480 | 0.9890 | 0.8910 | 0.9840 |
| 7 | 0.9772 | 0.8585 | 0.9898 | 0.8992 | 0.9850 |
| 8 | 0.9777 | 0.8640 | 0.9898 | 0.8995 | 0.9857 |
| 9 | 0.9780 | 0.8689 | 0.9896 | 0.8992 | 0.9861 |
| 10 | 0.9779 | 0.8579 | 0.9886 | 0.8694 | 0.9874 |
| 11 | 0.9744 | 0.8179 | 0.9904 | 0.8976 | 0.9815 |
| 12 | 0.9786 | 0.8759 | 0.9885 | 0.8804 | 0.9880 |
| 13 | 0.9779 | 0.8678 | 0.9889 | 0.8873 | 0.9867 |
| 14 | 0.9791 | 0.8685 | 0.9904 | 0.9036 | 0.9865 |
| 15 | 0.9575 | 0.7543 | 0.9780 | 0.7756 | 0.9753 |
| 16 | 0.9579 | 0.7655 | 0.9771 | 0.7690 | 0.9766 |

| Fold | $A_{cc}$ | $S_e$ | $S_p$ | $P^+$ | $P^-$ |
|---|---|---|---|---|---|
| 17 | 0.9696 | 0.8046 | 0.9856 | 0.8446 | 0.9811 |
| 18 | 0.9632 | 0.7675 | 0.9884 | 0.8950 | 0.9706 |
| 19 | 0.9671 | 0.7789 | 0.9887 | 0.8873 | 0.9750 |
| 20 | 0.9654 | 0.7672 | 0.9872 | 0.8681 | 0.9747 |
| 21 | 0.9668 | 0.7798 | 0.9864 | 0.8565 | 0.9772 |
| 22 | 0.9644 | 0.7555 | 0.9844 | 0.8225 | 0.9768 |
| Average | 0.9737 | 0.8329 | 0.9884 | 0.8802 | 0.9827 |

In the third experiment, a continuous uniform distribution[5] noise is added to each ECG segment for training and testing datasets to ascertain the model's robustness. Checking the classification integrity in a noisy environment is very important because noise distorts the ECG signal waveforms (Oliveira, Duarte, Abreu, & Vieira Filho, 2018). The respective results are shown in Figures 2 and 3, where the Signal-to-noise-ratio (SNR) is that from the test dataset.

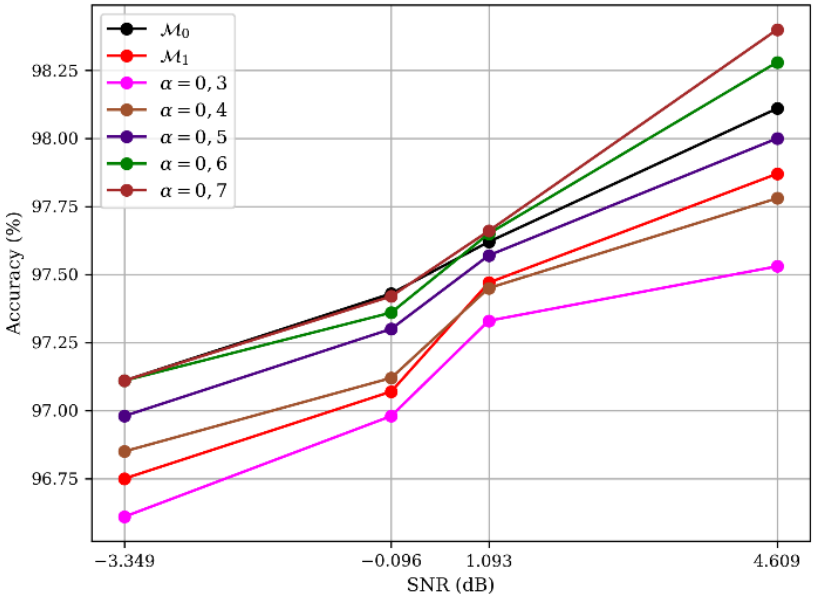


**Figure 2.** The accuracy obtained taking noise in training and testing datasets.

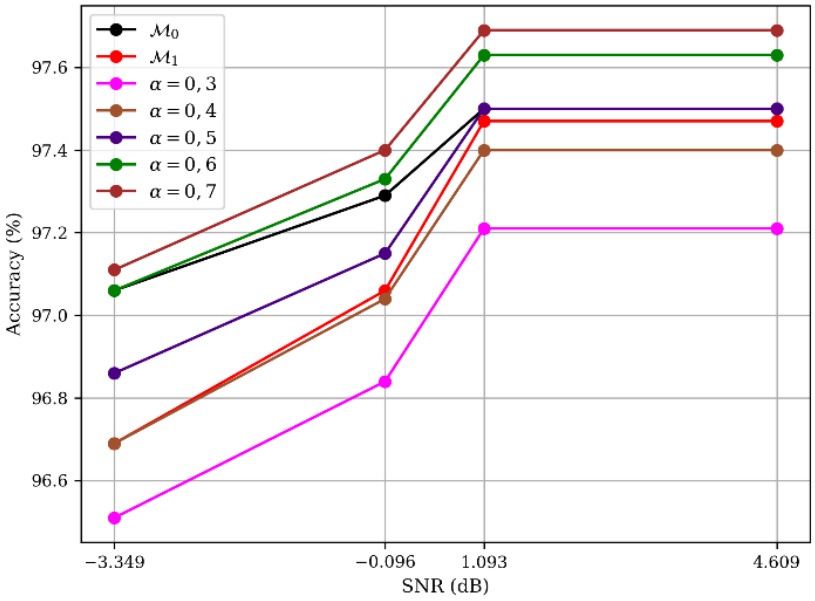


**Figure 3.** The accuracy obtained taking noise only in the testing dataset.

[5] Random real numbers in the interval $[0, 1)$.

Figure 4 illustrates a noiseless PVC heartbeat (Figure 4 (a)) and a noisy one (Figure 4 (b)). In Figures 4 (c) and (d), we have the low and high-frequency components obtained by applying the AMUSE method, respectively, where it can be noted that the lowest frequency components are less affected by noise. This shows an AMUSE advantage which is separating the noisy components providing a signal with better SNR. However, it is important to highlight that the estimated components are not on the same scale as the original signal and, in addition, they have a 180-degree lag. Even so, GNB algorithms can capture arrhythmic patterns.

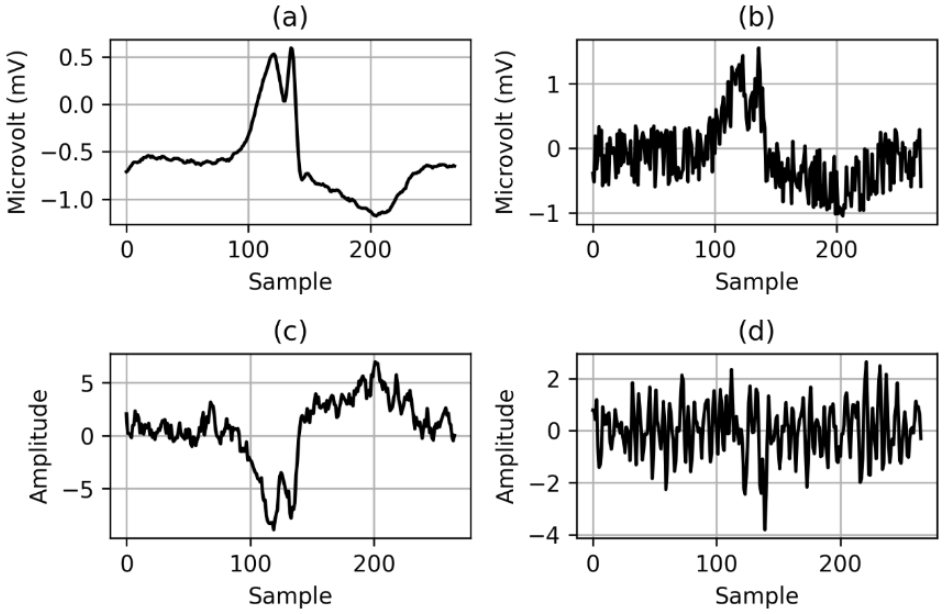


**Figure 4.** Examples of (a) noiseless PVC, extracted from the ECG register number 223, (b) noisy PVC; (c) and (d) AMUSE low and high-frequency components, respectively.

Robustness is also evaluated to detection errors in R peaks (or QRS) position[6]. In this experiment, a random deviation in the integer interval [−10,10] is added to the R peak actual location[7]. This implementation is necessary since the proposed approach is based on ECG segmentation which depends on the R wave position. The obtained results are shown in Table 5.

**Table 5.** Results take a deviation in the actual R peak location.

| Model | $A_{cc}$ | $S_e$ | $S_p$ | $P^+$ | $P^-$ |
|---|---|---|---|---|---|
| | | | Single models | | |
| $\mathcal{M}_0$ | 0.9710 | 0.8186 | 0.9845 | 0.8232 | 0.9840 |
| $\mathcal{M}_1$ | 0.9731 | 0.8577 | 0.9833 | 0.8190 | 0.9874 |
| | | | AHP ensemble approach | | |
| $\alpha = 0.3$ | 0.9676 | 0.8798 | 0.9753 | 0.7590 | 0.9892 |
| $\alpha = 0.4$ | 0.9747 | 0.9311 | 0.9820 | 0.8956 | 0.9885 |
| $\alpha = 0.5$ | 0.9747 | 0.8546 | 0.9853 | 0.8367 | 0.9871 |
| $\alpha = 0.6$ | 0.9763 | 0.8416 | 0.9882 | 0.8627 | 0.9860 |
| $\alpha = 0.7$ | 0.9775 | 0.8148 | 0.9918 | 0.8983 | 0.9838 |

Until here, experiments were performed for PVC and Normal classes. To evaluate the performance for other types of heartbeats, such as RBBB/LBBB, Atrial, and Ventricular Fibrillation, and others, the fourth experiment is executed by taking PVC as positive class and all other heartbeats as a negative class, considering all arrhythmias available in the databases used. This experimentation is important because RBBB/LBBB heartbeats can be confused with PVC as reported in the introduction. Furthermore, each class of arrhythmia has its particularities. Figure 5 (a) and (b) shown the PVC and LBBB heartbeats types, respectively, where some similarities in the waveforms can be observed: inverted QRS complex and prominent T wave. Results for this experiment are shown in Table 6.

[6] This position refers to occurrence of samples, considering entire ECG signal, related to maximum R wave value.
[7] Location available at MIT/BIH-ARDB.

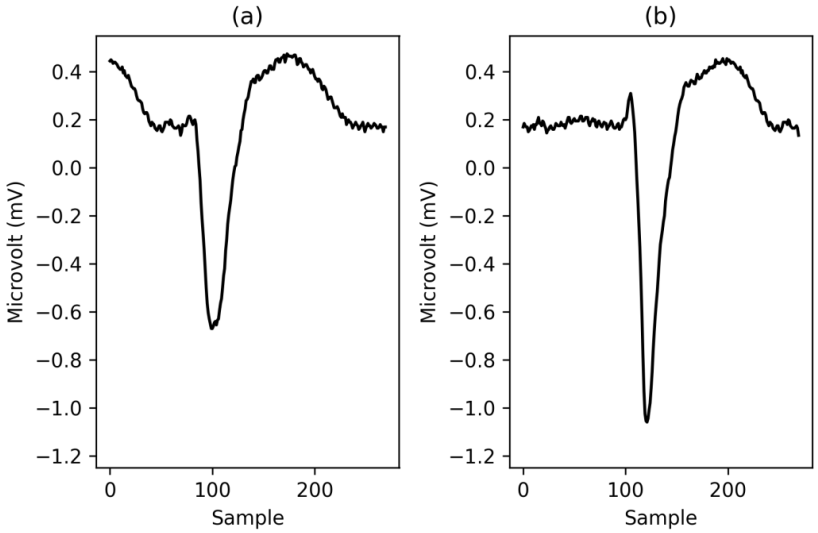


**Figure 5.** Examples of (a) PVC and (b) LBBB heartbeats from the ECG register number 207.

**Table 6.** Results for the PVC and all other types of heartbeats.

| Model | $A_{cc}$ | $S_e$ | $S_p$ | $P^+$ | $P^-$ |
|---|---|---|---|---|---|
| Single models | | | | | |
| $\mathcal{M}_0$ | 0.9702 | 0.8180 | 0.9804 | 0.7369 | 0.9877 |
| $\mathcal{M}_1$ | 0.9698 | 0.8596 | 0.9772 | 0.7167 | 0.9904 |
| AHP ensemble approach | | | | | |
| $\alpha = 0.3$ | 0.9596 | 0.8826 | 0.9648 | 0.6273 | 0.9919 |
| $\alpha = 0.4$ | 0.9654 | 0.8705 | 0.9718 | 0.6742 | 0.9911 |
| $\alpha = 0.5$ | 0.9714 | 0.8571 | 0.9791 | 0.7332 | 0.9903 |
| $\alpha = 0.6$ | 0.9766 | 0.8437 | 0.9855 | 0.7960 | 0.9895 |
| $\alpha = 0.7$ | 0.9814 | 0.8180 | 0.9923 | 0.8777 | 0.9878 |

Lastly, the AHP ensemble is compared to state-of-the-art approaches, taking the datasets according to Table 2. Comparative results are shown in Table 7.

**Table 7.** Comparison among the state-of-the-art methods and the proposed AHP ensemble.

| Approach | $A_{cc}$ | $S_e$ | $S_p$ | $P^+$ | Tr | Te |
|---|---|---|---|---|---|---|
| Liu et al. (2015) | 0.9890 | 0.9026 | - | 0.9890 | D3 | D4 |
| Proposed, $\alpha = 0.7$ | 0.9867 | 0.9058 | 0.9932 | 0.9146 | D3 | D4 |
| Li et al. (2014) | 0.9820 | 0.9310 | 0.9850 | 0.8140 | D1 | D2 |
| Zarei et al. (2016) | 0.9877 | 0.9612 | - | 0.8648 | D1 | D2 |
| Zhou et al. (2017) | 0.9941 | 0.9759 | 0.9954 | 0.9355 | D1 | D2 |
| Xie et al. (2019) | 0.9638 | 0.9788 | 0.9756 | 0.9546 | D1 | D2 |
| Oliveira et al. (2019) | 0.9840 | 0.9110 | 0.9870 | 0.8570 | D1 | D2 |
| Proposed, $\alpha = 0.7$ | 0.9875 | 0.9065 | 0.9946 | 0.9374 | D1 | D2 |
| Proposed, $\alpha = 0.3$ | 0.9802 | 0.9787 | 0.9818 | 0.9817 | D1 | D2 |
| Ebrahimzadeh and Khazaee (2010) | 0.9540 | - | - | - | D5 | D6 |
| Proposed, $\alpha = 0.7$ | 0.9869 | 0.9761 | 0.9877 | 0.8559 | D5 | D6 |
| Inan et al. (2006) | 0.9520 | 0.8520 | - | 0.9240 | D7 | D8 |
| Proposed, $\alpha = 0.7$ | 0.9957 | 0.9864 | 0.9965 | 0.9631 | D7 | D8 |
| Shen et al. (2011) | 0.9700 | - | - | - | D9 | D9 |
| Proposed,$\alpha = 0.7$ | 0.9878 | 0.9714 | 0.9925 | 0.9740 | D9 | D9 |

Tr and Te mean training and test dataset, respectively.

## Discussion

From results in Table 3, it is noted that the AHP ensemble approach is better than single models regardless of $\alpha$ probability, highlighting $P^+$ metric, which is 9.14% higher than the best single model result due to the greater number of true positives. On the other hand, from Table 4, it is observed that the results for different datasets, from the second row onwards, present inferior performance since ECG registers belonging to D1 and D2 datasets are good representations of the analyzed patterns. That's why most of the researches cited in the

introduction use these datasets in the training and testing phases. In general, taking into account average metrics, it is noted that more false alarms occur, mainly false positives. Hence, $P^+$ and $S_e$ metrics achieved the greatest reductions. This is because some ECG registers do not have PVC heartbeat instances. Anyway, on average, the accuracy is above 97%.

In addition to performance, the robustness of the proposed approach was also validated. The graph in Figure 2 makes it clear that poor SNR causes loss of performance. In this noisy environment, the AHP ensemble, with $\alpha = 0.4$, is better or equal to $\mathcal{M}_0$ single model, being superior as SNR increases. On the other hand, when noise is added only in the test dataset, the results presented in Figure 3 show that the AHP ensemble, with $\alpha = 0.4$ and $\alpha = 0.6$, is better regardless of SNR. Moreover, in this case, when SNR is greater than 1.093 dB, the performance stabilizes. These results are very important since the proposed approach does not implement a pre-processing step for noise attenuation.

Robustness was also validated for errors in the R peak detection. Comparing results between Tables 3 and 5, we noted a performance decrease for accuracy close to 1%, considering AHP with $\alpha = 0.7$. Again, the sharpest decrease occurs for PVC class, according to $P^+$ and $S_e$ metrics, since it has fewer instances, so it is more susceptible to changes in the attribute extraction step. However, for $S_e$, when $\alpha = 0.7$, there was an increase of around 1%. This is due to the weighted combination of the AHP ensemble approach since the metric $S_e$ for model $\mathcal{M}_1$ had a smaller decrease than that of the model $\mathcal{M}_0$.

As mentioned in the Introduction section, a PVC recognition method must differentiate among PVC and RBBB or LBBB, as there may be cases where these beats are similar, according to the example in Figure 5. The proposed approach has been tested for this ability. From results in Table 6, in comparison to the ones in Table 2, we noted decreases of 6.36% for $P^+$ and 9.76% for $S_e$ about $\alpha = 0.7$, when all other heartbeats were considered as negative class. Although these reductions in the performance are relevant, all metrics for $\alpha = 0.7$ are greater than 90%. An additional reason for these results is that RBBB and LBBB beats, for example, are only available for eight registers[8], and a patient ECG register is considered in the training or testing phase, but not for both.

In comparison to the state-of-the-art methods, Table 7, regarding D3 and D4 datasets, it is noted that the proposed approach surpassed the approach of Liu et al. (2015) only in $S_e$ metric, with lower performance for $A_{cc}$ and $P^+$, implying that the number of false negatives is greater for the proposed approach.

To the results obtained from D1 and D2 datasets, the proposed approach with $\alpha = 0.7$ surpasses all state-of-the-art methods concerning $S_p$, except for the one proposed by Zhou et al. (2017). For $P^+$ metric, the proposed approach also outperformed the other methods but not the one proposed by Xi et al. (2019). Such results indicate that the proposed approach generates less false positives but, on the other hand, it generates more false negatives when $\alpha = 0.7$. For results with $\alpha = 0.3$, it is noticed that accuracy is lower, but, unlike the previous case, $S_e$ is greater than other methods, except the one proposed by Xi et al. (2019). These results imply a reduction in false negatives by taking a lower α cut-off probability. Therefore, the proposed approach allows us to choose which performance metric we will emphasize, which implies more false positives or negatives.

When comparing D5 and D6 datasets, the proposed approach surpassed Ebrahimzadeh and Khazaee (2010) concerning accuracy. In the fourth comparison, implemented on D7 and D8 datasets, the proposed approach is superior to the method presented in Inan et al. (2006) concerning all metrics. In fact, the model induced on these datasets generated the best performance results in comparison to all others, except for $P^+$.

In the last comparison, over the D9 dataset, the proposed approach is better than one proposed by Shen et al. (2011).

The proposed approach was better or worse in the above comparisons depending on the dataset and cut-off probabilities, obtaining greater results for most metrics and comparisons. It is also evident that the proposed approach generated high $S_e$ and $P^+$ values, greater than 0.9, except for the implementation over D5 and D6 datasets, where it was obtained a reduced $P^+$, resulting in fewer occurrences of false positives and false negatives. Another advantage of the proposed approach is that it does not include a pre-processing step to eliminate noise, as the other approaches, which reduces the computational load.

## Conclusion

This work proposes a new approach aiming at PVC recognition based on the AMUSE components with linear combination and GNB models, which are combined in ensemble learning weighted by AHP. Several experiments were performed, including cross-validation, noisy environment, many arrhythmia types, and

[8] ECG registers that have RBBB or LBBB heartbeats are: 109, 111, 118, 207, 212, 214, 231, 232.

comparisons with baseline methods. Obtained results showed good performance for the propositions varying a cut-off probability in the AHP ensemble. In comparison to other methods, the proposed approach was better in most of the cases. The best performance was obtained when considering the use of D7 and D8 datasets, consisting 99.57% accuracy, 98.64% sensitivity, and 99.65% specificity. Besides that, the proposed approach has a lower computational load since there is no need for the pre-processing stage, and it is based on the Naive Bayes concept, which depends only on the probabilities computation.

Future works include research on conversion functions for the AHP and other scales and more in-depth investigations into how noise affects performance. In addition, implementation of testing and training phases in other databases.

## Acknowledgements

This study was financed in part by the Coordenação de Aperfeiçoamento de Pessoal de Nível Superior - Brasil (CAPES) - Finance code 001.

## References

Adnane, M., & Belouchrani, A. (2013). Premature ventricular contraction arrhythmia detection using wavelet coefficients. In *Proceedings of the 2013 8th International Workshop on Systems, Signal Processing and their Applications* [WoSSPA], (p. 170-173). DOI: https://doi.org/10.1109/WoSSPA.2013.6602356

Ahn, M.-S. (2013). Current concepts of premature ventricular contractions. *Journal of Lifestyle Medicine, 3*(1), 26-33.

Bazi, Y., Hichri, H., Alajlan, N., & Ammour, N. (2013). Premature ventricular contraction arrhythmia detection and classification with gaussian process and S-transform. In *Proceedings of the 2013 Fifth International Conference on Computational Intelligence, Communication Systems and Networks*, (p. 36-41). DOI: https://doi.org/10.1109/CICSYN.2013.44

Bennett, D. H. (2012). *Bennett's cardiac arrhythmias: practical notes on interpretation and treatment*. Hoboken, NJ: John Wiley & Sons.

Cha, Y.-M., Lee, G. K., Klarich, K. W., & Grogan, M. (2012). Premature ventricular contraction-induced cardiomyopathy: a treatable condition. *Circulation: Arrhythmia and Electrophysiology, 5*(1), 229-236. DOI: https://doi.org/10.1161/CIRCEP.111.963348

Oliveira, B. R., Duarte, M. A. Q., & Vieira Filho, J. (2022). Early detection of Ventricular Bigeminy/Trigeminy rhythms. *Multi-Science Journal*, *5*(1), 1-10. DOI: https://doi.org/10.33837/msj.v5i1.1525

Ebrahimzadeh, A., & Khazaee, A. (2010). Detection of premature ventricular contractions using MLP neural networks: a comparative study. *Measurement, 43*, 103-112. DOI: https://doi.org/10.1016/j.measurement.2009.07.002

Garcia, T. B., & Miller, G.T. (2004). *Arrhythmia recognition: the art of interpretation*. New York, NY: Jones & Bartlett.

Goldberger, A. L., Amaral, L. A. N., Glass, L., Hausdorff, J. M., Ivanov, P. C., Mark, R. G., ... Stanley, H. E. (2000). Physiobank, physio toolkit, and physionet: components of a new research resource for complex physiologic signals. *Circulation, 101*(23), e215–e220. DOI: http://doi.org/10.1161/01.CIR.101.23.e215

Hadia, R., Guldenring, D., Finlay, D. D., Kennedy, A., Janjua, G., Bond, R., & McLaughlin, J. (2017). Morphologybased detection of premature ventricular contractions. *2017 Computing in Cardiology - CinC*, 1-4. DOI: https://doi.org/10.22489/CinC.2017.211-260

Hall, J. E. (2015). *Guyton and hall textbook of medical physiology e-Book* (12a ed.). New York, NY: Elsevier Health Sciences.

Ho, W., & Ma, X. (2018). The state-of-the-art integrations and applications of the analytic hierarchy process. *European Journal of Operational Research, 267*(2), 399-414. DOI: https://doi.org/10.1016/j.ejor.2017.09.007

Huizar, J. F., Fisher, S. G., Ramsey, F. V., Kaszala, K., Tan, A. Y., Moore, H., ... Singh, S. N. (2021). Outcomes of premature ventricular contraction–cardiomyopathy in the veteran population: a secondary analysis of the CHF-STAT Study. *JACC: Clinical Electrophysiology, 7*(3), 380-390. DOI: http://doi.org/10.1016/j.jacep.2020.08.028

Inan, O. T., Giovangrandi, G., & Kovacs, G. T. A. (2006). Robust neural-network-based classification of premature ventricular contractions using wavelet transform and timing interval features. *IEEE Transactions on Biomedical Engineering, 53*(12), 2507-2515. DOI: http://doi.org/10.1109/TBME.2006.880879

Kim, Y. G., Han, K.-D., Choi, J.-I., Choi, Y. Y., Choi, H. Y., Shim, J., & Kim, Y. H. (2021a). Premature ventricular contraction is associated with increased risk of atrial fibrillation: a nationwide population-based study. *Scientific Reports, 11*(1601), 1-8. DOI: https://doi.org/10.1038/s41598-021-81229-0

Kim, Y. G., Choi, Y. Y., Han, K.-D., Min, K. J., Choi, H. Y., Shim, J., ... Kim, Y.-H. (2021b). Premature ventricular contraction increases the risk of heart failure and ventricular tachyarrhythmia. *Scientific Reports, 11*(12698). DOI: https://doi.org/10.1038/s41598-021-92088-0

Kusumoto, F. M. (2009). *ECG Interpretation: from pathophysiology to clinical application*. New York, NY: Springer.

Latchamsetty, R., & Bogun, F. (2015). Premature ventricular complexes and premature ventricular complex induced cardiomyopathy. *Current Problems in Cardiology, 40*(9), 379-422. DOI: https://doi.org/10.1016/j.cpcardiol.2015.03.002

Li, P., Liu, C., Wang, X., Zheng, D., Li, Y., & Liu, C. (2014). A low-complexity data-adaptive approach for premature ventricular contraction recognition. *Signal, Image and Video Processing, 8*(1), 111-120. DOI: https://doi.org/10.1007/s11760-013-0478-6

Liu, X., Du, H., Wang, G., Zhou, S., & Zhang, H. (2015). Automatic diagnosis of premature ventricular contraction based on lyapunov exponents and LVQ neural network. *Computer Methods and Programs in Biomedicine, 122*, 47-55. DOI: https://doi.org/10.1016/j.cmpb.2015.06.010

Mika, S., Ratsch, G., Weston, J., Scholkopf, B., & Mullers, K. R. (1999). Fisher discriminant analysis with kernels, Neural Networks for Signal Processing IX: In *Proceedings of the 1999 IEEE Signal Processing Society Workshop (Cat Nº98TH8468)*, (p. 41-48). DOI: http://doi.org/10.1109/NNSP.1999.788121

Oliveira, B. R. d., Abreu, C. C. E. d., Duarte, M. A. Q., & Vieira Filho, J. (2019). Geometrical features for premature ventricular contraction recognition with analytic hierarchy process based machine learning algorithms selection. *Computer Methods and Programs in Biomedicine, 169*, 59–69. DOI: https://doi.org/10.1016/j.cmpb.2018.12.028

Oliveira, B. R. d., Duarte, M. A. Q., Abreu, C. C. E. d., & Vieira Filho, J. (2018). A wavelet-based method for power-line interference removal in ECG signals. *Research on Biomedical Engineering, 34*(1), 73-86. DOI: https://doi.org/10.1590/2446-4740.01817

Oliveira, B. R. d., Oliveira, A. R. d., Freitas, A. P. C. d., & Duarte, M. A. Q. (2021). A tool for the analytic hierarchy process based on Leibniz's formula for determinants computation. *Revista Eletrônica Paulista de Matemática, 20*, 12–21. DOI: https://doi.org/10.21167/cqdvol20202123169664broaroapcfmaqd1221

Saaty, R. W. (1987). The analytic hierarchy process - what it is and how it is used. *Mathematical Modelling, 9*(3-5), 161-176. DOI: http://doi.org/10.1016/0270-0255(87)90473-8

Santos, P. H. d., Neves, S. M., Sant'Anna, D. O., Oliveira, C. H. d., & Carvalho, H. D. (2019). The analytic hierarchy process supporting decision making for sustainable development: an overview of applications. *Journal of Cleaner Production, 212*, 119-138. DOI: https://doi.org/10.1016/j.jclepro.2018.11.270

Shen, Z., Hu, C., Li, P., & Meng, M. Q. H. (2011). Research on premature ventricular contraction real-time detection based support vector machine. In *Proceedings of the 2011 IEEE International Conference on Information and Automation*, (p. 864-869). DOI: https://doi.org/10.1109/ICINFA.2011.5949116

Tong, L., Liu, R.-W., Soon, V. C., & Huang, Y. F. (1991). Indeterminacy and identifiability of blind identification. *IEEE Transactions on Circuits and Systems, 38*(5), 499-509. DOI: https://doi.org/10.1109/31.76486

Xie, T., Li, R., Shen, S., Zhang, X., Zhou, B., & Wang, Z. (2019). Intelligent analysis of premature ventricular contraction based on features and random forest. *Journal of Healthcare Engineering, 2019*(5787582). DOI: https://doi.org/10.1155/2019/5787582

Zarei, R., He, J., Huang, G., & Zhang, Y. (2016). Efective and efficient detection of premature ventricular contractions based on variation of principal directions. *Digital Signal Processing, 50*, 93-102. DOI: https://doi.org/10.1016/j.dsp.2015.12.002

Zhou, F.-Y., Jin, L.-P., & Dong, J. (2017). Premature ventricular contraction detection combining deep neural networks and rules inference. *Artificial Intelligence in Medicine, 79*, 42-51. DOI: http://dx.doi.org/10.1016/j.artmed.2017.06.004